Research Square

Preprints are preliminary reports that have not undergone peer review.
They should not be considered conclusive, used to inform clinical practice,
or referenced by the media as validated information.

An Integrated Risk Assessment Framework for Overburden Dump Slopes in Opencast Mines: Coupled Deterministic–Probabilistic Stability Analysis and Physico-Chemical Characterisation — Field Evidence from the Jharia Coalfield, India

JOBA GOSWAMI

joba.goswami21@gmail.com

Indian Institute of Technology Dhanbad

MRINALJYOTI ADHYAPOK

Jorhat engineering college, Asssam Science and technology university, Assam

Biswajit Paul

Indian Institute of Technology Dhanbad

Research Article

Keywords: overburden dump, mine waste geohazard, slope stability, integrated risk assessment, reliability-based design, limit equilibrium, finite element, Monte Carlo simulation, probability of failure, reclamation, Jharia coalfield

Posted Date: March 12th, 2026

DOI: https://doi.org/10.21203/rs.3.rs-9031234/v1

License: This work is licensed under a Creative Commons Attribution 4.0 International License. Read Full License

Additional Declarations: No competing interests reported.

Abstract

Overburden (OB) dump failures in opencast mines represent a persistent geotechnical and environmental hazard in coal-producing nations worldwide, yet an integrated risk assessment framework coupling geomechanical stability, parametric uncertainty quantification, and post-mining land-quality assessment remains largely absent from the mine waste literature. This paper develops and demonstrates such a framework through a field investigation of OB dump slopes in the Eastern Jharia Coalfield (JCF), India. The approach integrates: (i) comprehensive physico-chemical characterisation of dump fill material, (ii) deterministic stability modelling using five Limit Equilibrium Method (LEM) formulations (Bishop Simplified, Morgenstern–Price, Janbu Simplified, Janbu Corrected, Spencer) in SLIDE 6.0 and Finite Element / Strength Reduction Method (FEM/SRM) analysis in FLAC/Slope 8.0, and (iii) full probabilistic risk quantification via Monte Carlo Simulation (MCS, n = 100,000) and First-Order Second-Moment (FOSM) analysis. The framework yields not only a probability of failure (P^f) and reliability index (β), but also a practitioner-oriented design chart linking β to mean FOS across a range of coefficient-of-variation values — a directly transferable tool for mine operators and regulatory bodies. Application to the JCF slope confirms critical instability across all methods: minimum FOS of 0.751 by LEM, 0.810 by FEM, and P^f of approximately 98% (β = −2.29; FOSM-derived, negative sign confirming mean FOS lies on the failure side of the limit state) from MCS — well above the commonly cited 2.3% threshold corresponding to β_target = 2.0, confirming near-certain failure under current geometric and material conditions. Friction angle governs sensitivity, while cohesion offers the most cost-efficient remediation pathway. The framework is designed to be replicable at any OB dump site globally, requiring only standard site investigation data, and is directly applicable to emerging mine-closure and reclamation planning requirements. The dump material (USCS: SP, slightly acidic, negligible cohesion, trace heavy-metal contamination including anomalous mercury linked to subsurface mine fires) is concurrently assessed for reclamation suitability, illustrating the integrated geotechnical-environmental utility of the approach.

1. Introduction

Coal still accounts for more than half of India's primary energy consumption, and that dependence shows no sign of easing. The country holds the world's fourth-largest coal reserves and ranks third globally in production, with opencast operations contributing around 83% of annual output [17, 36]. Every tonne of coal extracted from an opencast pit comes with a roughly equivalent volume of fragmented rock and soil—what the industry calls overburden—that has to be deposited on the surface. These waste piles, or OB dumps, can accumulate to considerable heights when mine operators face pressure to keep excavators and draglines moving. The predictable result is a landscape of steep,

unconsolidated slopes built from heterogeneous material whose geotechnical properties rarely receive the level of scrutiny applied to, say, an embankment dam [15, 16].

The consequences have been severe. In 2008, the Jayant (NCL) dump failure swept away a 135 m × 70 m section of slope and killed five workers; a year later, the Sesti (WCL) collapse—a 73-metre-high dump—buried two excavators and cost two more lives; and the 2016 Lalmatia (ECL) event buried both people and machinery with minimal prior warning [41]. Similar episodes have been recorded internationally, including the South Field lignite mine in Greece [14] and the 2013 Bingham Canyon slide in Utah, which displaced 65–70 million cubic metres of material [16]. What stands out about the Indian cases isn't simply that they occurred, but that slope angles were being held at 35°–40° or steeper in near-cohesionless fill—conditions where a factor of safety at or below 1.0 could have been anticipated from first principles.

Limit Equilibrium Methods (LEM) have served as the workhorse of geotechnical slope analysis for decades [7, 8, 9, 10]. The various formulations differ in how they handle inter-slice forces, and their comparative accuracy for homogeneous circular failure surfaces has been studied extensively—most notably by Fredlund & Krahn [11]. Finite Element approaches, particularly Strength Reduction Methods (SRM), provide a useful complement: instead of constraining failure to a predetermined slip surface, they let the failure mechanism develop naturally through progressive strain localisation [12, 13, 24]. The two families of methods typically agree reasonably well for simple geometries, though FOS discrepancies of 5–15% are not uncommon [12].

What neither of these deterministic approaches can easily communicate is how much confidence should accompany a calculated FOS. Field-measured shear strength parameters carry significant uncertainty—coefficients of variation (CoV) of 5–15% for friction angle and 20–40% for cohesion are typical for mine spoil [1, 28]. A computed FOS of, say, 0.77 could correspond to a probability of failure anywhere from a few percent to above 30%, depending on how the input distributions are spread [29]. Probabilistic methods, developed through the work of Cornell [6], Wu & Kraft [2], Alonso [3], Tang et al. [4], Vanmarcke [5], and formalised by Christian et al. [28], translate that uncertainty into a reliability index β and probability of failure Pf—quantities far more useful for risk management than a single deterministic number.

Despite this, probabilistic assessments of OB dump slopes remain uncommon, not only in India but across the broader mine waste literature. Most published studies—including the widely cited case studies by Kainthola et al. [15], Rai & Mahapatra [32], and Poulsen et al. [16]—stop at the deterministic FOS. To our knowledge, few have combined full physico-chemical fill characterisation with multi-method deterministic stability analysis and Monte Carlo–based probabilistic risk quantification into a single, replicable framework suited to

the mine waste context. The present study aims to address that gap. Working from original field samples and direct shear data from the Eastern JCF, we report: (i) a complete physico-chemical characterisation relevant to both stability and reclamation; (ii) deterministic LEM and FEM stability analyses; (iii) parametric sensitivity studies on cohesion and friction angle; and (iv) Monte Carlo–based probabilistic analysis yielding P^f and β with a supporting design chart. The framework is structured to be directly replicable at any OB dump site where standard site investigation data are available.

2. Study Area and Geological Context

The Jharia Coalfield covers roughly 453 km² of Dhanbad District in Jharkhand, bounded by latitudes 23°39'N–23°48'N and longitudes 86°11'E–86°27'E. By a wide margin, it is India's most important source of prime coking coal: 49 named seams have been worked here since the East India Company opened commercial operations on the Damodar River in 1774, and the field has been studied scientifically at least since Sengupta's [36] stratigraphic revision in 1980. The coal measures rest on Archaean metamorphic basement—granites and mica schists—and the overlying Gondwana succession alternates sandstone, shale, and carbonaceous horizons [36].sedimentary succession is Gondwana in age, comprising alternating sandstone, shale, and carbonaceous horizons [36].

Any honest account of the JCF has to acknowledge that the field has been heavily over-exploited. Around 70 underground mine fires are currently active across 17.32 km² of the coalfield, locking up an estimated 636 Mt of coking coal and 1,238 Mt of non-coking coal [36]. Surface subsidence from old goafs, spontaneous combustion, and the progressive failure of unreclaimed external dumps are the most visible legacies of more than a century of intensive—and not always well-regulated—mining.

The OB dump slope examined here is an external waste dump at the periphery of an active opencast complex in the eastern JCF. It was built by progressive end-tipping: trucks deposited waste over the crest, and the slope face advanced outward as the dump grew. This construction method, though operationally convenient, consistently produces steep, poorly consolidated slope faces with minimal inter-layer bonding [15, 25]. At the time of the September 2017 sampling campaign, slope angle in the working section ranged from roughly 35° to 38°, with vertical height between 12 and 18 m. There was no surface drainage channel at either the crest or the toe, and rilling scars on the face pointed to active erosion.

3. Materials and Methods

3.1 Sample Collection and Laboratory Testing

Soil samples were taken from three locations along the dump profile—top, middle, and lower horizon—using a manually operated split-tube coring tool (sampling depth 0–20 cm), following IS:2720 (Part IV)–1985. It should be acknowledged that 0–20 cm sampling captures only the near-surface portion of a dump whose failure surface most likely develops at depth (5–15 m below crest); the assumption that surface samples reflect bulk material properties rests primarily on the remarkable compositional uniformity observed across all three locations (see Fig. 9). Rotary coring in future investigations would let this assumption be tested directly. Sampling was conducted in September 2017, near the end of the monsoon season, when pore water pressures in the dump were expected to be near their seasonal peak. Samples were sealed on-site in polyethylene bags and transported to the authors' laboratory.

Although sampling was timed to capture near-peak monsoon moisture conditions, the stability analyses were conducted assuming zero excess pore water pressure—that is, dry or moist unsaturated conditions. Three reasons support this choice. First, no piezometric data were available from instrumented standpipes or vibrating-wire piezometers within the dump body; assigning an ru value without measured pore pressure profiles would introduce false precision rather than genuine rigour. Second, the freely draining SP-classified material ($cu \geq 80\%$, $D30 = 0.70–0.75$ mm) has high enough hydraulic conductivity to prevent sustained perched water tables during typical inter-event drainage periods—consistent with published drainage-rate estimates for similar coal-measure waste fills [21, 22]. Third, and most importantly: even under dry conditions—the most mechanically favourable scenario, giving the highest possible FOS—the computed value of approximately 0.76 already indicates failure. Positive pore-water pressures during monsoon infiltration would further reduce FOS and increase Pf above the already near-certain values reported here. The dry-condition analysis is therefore a best-case upper bound on FOS, not a conservative lower bound; actual stability during or after rainfall events is worse than the figures in this paper. Transient seepage modelling coupled to a rainfall-infiltration analysis is identified as a priority for future work (Section 8).

After air-drying, samples were disaggregated in a mortar, passed through a 2 mm mesh sieve, and split by coning and quartering before analysis. The test programme covered: particle size distribution by dry sieving (IS:2720 Part IV); consolidated-drained (CD) direct shear at normal stresses of 50, 100, and 150 kPa (IS:2720 Part XIII); specific gravity by density bottle (IS:2720 Part III); bulk density and gravimetric moisture content; pH and electrical conductivity by electrometric methods; water holding capacity by the perforated-dish procedure; and trace heavy metal concentrations (Cd, Pb, Zn, Hg) by Atomic Absorption Spectroscopy (AAS). Young's modulus for the FEM model was estimated from standard reference tables for SP-classified granular material [40], taking 30–50 MPa for medium-dense conditions.stresses of 50, 100 and 150 kPa (IS:2720 Part XIII); specific gravity by density bottle (IS:2720 Part III); bulk density and gravimetric moisture content;

pH and electrical conductivity (EC) by electrometric methods; water holding capacity by the perforated-dish (Keen box) procedure; and trace heavy metal concentrations (Cd, Pb, Zn, Hg) by Atomic Absorption Spectroscopy (AAS). Young’s modulus for FEM modelling was estimated from standard reference tables for SP-classified granular material [40], taking 30–50 MPa for medium-dense conditions.

3.2 Deterministic Slope Stability Analysis

3.2.1 Limit Equilibrium Methods

The five LEM formulations used here represent the standard toolkit of practising geotechnical engineers [11, 35]. All share the same basic architecture: the potential failure mass is divided into vertical slices, and equilibrium equations are applied to each slice to back-calculate the factor of safety—the ratio of available shear strength to mobilised shear stress. The methods differ principally in the inter-slice force assumptions they invoke to make the otherwise statically indeterminate problem tractable. Bishop's Simplified method [7] satisfies moment equilibrium only and assumes zero inter-slice shear, a simplification that works well for circular slip surfaces. Janbu's Simplified formulation [10] satisfies force equilibrium; the Corrected variant adds an empirical correction factor to partially compensate for neglected shear forces—an important distinction for flatter, elongated failure surfaces. Both Morgenstern–Price [8] and Spencer [9] satisfy full equilibrium; the key difference is that Morgenstern–Price allows the inter-slice force function to vary along the slip surface, whereas Spencer assumes it constant (making a constant-function Morgenstern–Price analysis numerically equivalent to Spencer [11]). All analyses were run in SLIDE 6.0 (Rocscience Inc.), with the critical slip surface located by a grid search over circular arcs.

$$FOS = \tau_f / \tau = (c' + \sigma'_n \cdot \tan \varphi') / \tau$$

where c' and φ' are the effective strength parameters and σ'_n is the effective normal stress on the failure plane. The methods differ principally in the inter-slice force assumptions they invoke to make the otherwise statically indeterminate problem tractable. Bishop's Simplified method [7] satisfies moment equilibrium only and assumes zero inter-slice shear, a simplification that works well for circular slip surfaces. Janbu's Simplified formulation [10] satisfies force equilibrium; the Corrected variant adds an empirical correction factor to partially compensate for the neglected shear forces — an important distinction for flatter, elongated failure surfaces. Both the Morgenstern–Price [8] and Spencer [9] methods satisfy full equilibrium and are generally regarded as the most rigorous of the slice approaches; the key difference is that Morgenstern–Price allows the inter-slice force function to vary along the slip surface, whereas Spencer assumes it constant (making a Morgenstern–Price analysis with a constant function numerically

equivalent to Spencer [11]). All analyses were performed in SLIDE 6.0 (Rocscience Inc.), with the critical slip surface located by a grid search over circular arcs.

3.2.2 Finite Element / Strength Reduction Method

The FEM analysis used FLAC/Slope 8.0 (ITASCA Consulting Group) with a Mohr–Coulomb constitutive model. Under the SRM, shear strength parameters are progressively reduced by a common trial factor F until the model can no longer find an equilibrium state, at which point F equals the factor of safety [12, 13]. One advantage of the SRM is that it imposes no prior assumption about the shape or location of the critical failure surface—the failure mechanism emerges from the stress analysis itself. For the present slope, the geometry is simple enough that a near-circular mechanism was anticipated and confirmed. Elastic parameters for the FEM model ($E = 40$ MPa, $\nu = 0.30$) are consistent with medium-dense SP sand [25].

$c_{trial} = c' / F \; ; \; \tan \varphi_{trial} = \tan \varphi' / F$

Dilation was computed as $\psi = (2/3)\varphi'$ for $\varphi' > 30°$, following the partially-associated flow rule applied in comparable coal-measure granular fill modelling [12]. This yields $\psi \approx 22°$ for the present material. To confirm that this assumption doesn't drive the result, the FEM analysis was also run with $\psi = 0°$ (non-associative, appropriate for loose fills), which returned $FOS = 0.803$—less than 1% different from the $\psi = (2/3)\varphi'$ result. The stability conclusion is therefore insensitive to the dilation assumption for this geometry.

3.3 Probabilistic Analysis

3.3.1 Monte Carlo Simulation

Direct Monte Carlo Simulation [1, 28, 29] is arguably the most transparent probabilistic approach for slope stability. The procedure is conceptually simple: sample each uncertain input parameter from its assumed probability distribution, compute the resulting FOS, and repeat N times. The probability of failure is then estimated as $P^f = N(FOS < 1.0) / N_{total}$. Here N was set to 100,000 for the combined-parameter case (10,000 for single-parameter sensitivity runs), which is sufficient to resolve Pthis study N was set to 100,000 for the combined-parameter case (10,000 for single-parameter sensitivity runs), which is sufficient to resolve P^f values down to approximately 0.001% with reasonable precision [29]. Input distributions were assumed normal, with CoV values drawn from published literature (Malkawi et al. [1] and Christian et al. [28]) because the $n = 3$ sample dataset is statistically insufficient to estimate CoV independently. The sample-derived CoV for φ' is $\sigma\varphi/\mu\varphi = 1.0°/33.5° \approx 3\%$, compared to the literature-based value of 6% [1, 37] used in the MCS. A sensitivity check at the sample-derived CoV of 3% yields $P_f > 99.99\%$, confirming that the lower CoV makes the instability conclusion stronger, not weaker. The adopted

values are: φ' CoV = 6% (direct shear on granular material), c' CoV = 33% (highly uncertain near-zero cohesion), γ CoV = 5%. The closed-form Bishop Simplified expression was used within each trial to keep the simulation computationally tractable.

The choice of normal distributions for φ', c', and γ, and the assumption of statistical independence among them, deserves explanation. Normal distributions follow established precedent: Christian et al. [28] and Phoon & Kulhawy [37] both show that, for granular soils characterised by direct-shear testing, the normal distribution fits observed data adequately, and that MCS output (P_f and β) is relatively insensitive to moderate departures from normality when CoV stays below roughly 20%. Lognormal distributions, which enforce positivity and are sometimes preferred for c' when that parameter can span zero, would be more theoretically appropriate for cohesion; in practice, since the measured c' here is effectively zero (0.1–0.2 kPa), the distinction is immaterial. The available dataset is too small to discriminate between distribution families on statistical grounds. A brief check replacing the normal assumption for φ' with a lognormal of identical mean and CoV shifted P_f by less than 0.4 percentage points, confirming distribution-robustness. The independence assumption—no correlation between φ', c', and γ—is adopted for transparency and reproducibility in the absence of defensible correlation data.

3.3.2 First-Order Second-Moment Method and Reliability Index

The FOSM approach [6, 28] offers a less computationally intensive alternative to direct simulation. It approximates FOS variance through a first-order Taylor expansion about the mean values of the input variables.

$$\sigma_{FOS} \approx \Sigma_i \left(\partial FOS/\partial x_i\right) \cdot \sigma_{x_i}$$

The reliability index $\beta = (\mu_{FOS} - 1.0) / \sigma_{FOSM}$ [4, 6, 26] describes how many standard deviations the mean FOS lies from the failure threshold, where σ_{FOSM} is the FOSM-estimated standard deviation of FOS (distinct from σ_{MCS}, the MCS-sampled standard deviation—see § 5.1). When $\mu_{FOS} < 1.0$, β is negative, meaning the mean itself sits on the failure side of the limit state; the magnitude |β| indicates how far below the threshold. Throughout this paper β is reported with its correct sign—negative values confirm the expected FOS is below unity. Christian et al. [28] recommend $\beta \geq 2.0$–4.0 for slopes in the safe domain; at $\beta = -2.29$, the present slope sits 2.29 standard deviations below the failure threshold—confirming near-certain failure. Under DGMS guidance [34], the minimum acceptable design FOS is 1.3; when parametric uncertainty is explicitly accounted for, meeting this requirement while achieving an acceptable β demands a mean FOS considerably above 1.3, as shown in the design chart (Fig. 8).

4. Results

4.1 Physico-Chemical Character of the OB Fill

Table 1 sets out the measured physico-chemical properties. pH readings of 5.85–6.50 place all three samples in the slightly acidic range—unsurprising given the carboniferous sedimentary lithology of the JCF, which tends to produce mildly acidic weathering products [36]—but the implications for post-mining land use are significant. Brady & Weil [38] identify 6.5–7.5 as optimal for most crop species; below that threshold, nitrogen, phosphorus, and potassium become progressively less available, and phytotoxic metals such as aluminium and manganese become more soluble. In practice, the dump surface left unattended won't support meaningful vegetation cover—removing one of the simplest passive reinforcement mechanisms for shallow slope stabilisation.of the JCF overburden tends to produce mildly acidic weathering products [36] — but the consequence for post-mining land use is significant. Brady & Weil [38] established the 6.5–7.5 range as optimal for most crop species; below that threshold, nitrogen, phosphorus, and potassium become progressively less available, and phytotoxic metals, particularly aluminium and manganese, become more soluble. In practice this means that the dump surface, left unattended, will not support meaningful vegetation cover — which in turn removes one of the simplest passive reinforcement mechanisms available for shallow slope stabilisation.

Bulk density at 1.58 ± 0.20 g/cc reflects the dump's compaction history. Heavy earth-moving machinery (HEMM)—the 90-tonne dump trucks and tracked excavators working on and near the dump surface—produces localised compaction that modestly increases friction angle but also creates an impermeable surface crust, redirecting infiltrating rainwater laterally rather than allowing vertical drainage [31]. The measured water holding capacity of 28–30% is low, consistent with the coarse-sand-dominant texture, and electrical conductivity at 0.04 dS/m sits well below Saxena's [39] 4 dS/m threshold for adverse effects on plant establishment.

Heavy metal concentrations (Cd: 0.014 mg/kg; Pb: 0.3 mg/kg; Zn: 0.321 mg/kg; Hg: 5.414 mg/kg), determined by acid-digest AAS on dry-weight samples, merit attention. Mercury in particular stands out: the measured level is substantially elevated relative to typical uncontaminated soil backgrounds (0.01–0.3 mg/kg; WHO soil reference). This likely reflects partial combustion of carbonaceous material within the dump, a secondary process frequently observed in Jharia where subsurface mine fires drive upward heat and gas flux through the overburden [36]. Elevated mercury suppresses photosynthetic efficiency and represents a long-term reclamation challenge extending well beyond the immediate slope stability problem.

Table 1
Physico-chemical properties of OB dump samples (Eastern JCF).

Sl.	Parameter	Measured Values	Remarks
1	pH	6.45 / 5.85 / 6.50	Slightly acidic; limits nutrient availability
2	Electrical Conductivity	0.04 dS/m	Well within acceptable range
3	Water Holding Capacity	28–30%	Low; poor moisture retention
4	Specific Gravity	2.27–2.42	Within normal range for sandstone-derived fill
5	Bulk Density	1.58 ± 0.20 g/cc	Medium; reflects HEMM compaction
6	Moisture Content	2.46–2.48%	Very low; unsaturated conditions

4.2 Particle Size Distribution and Strength Parameters

All three samples classify as Poorly Graded Sand (SP) under the Unified Soil Classification System (Table 2; Fig. 1). Coarse sand (> 1.18 mm) accounts for 42–48% of the mass in each case, fine sand for 22–24%, and the fines fraction (< 0.075 mm) is essentially absent. Uniformity coefficients between 7.75 and 8.04 suggest some gradation spread, but near-zero curvature coefficients (0.35–0.45, against the well-graded criterion of 1–3) confirm the SP classification. In practice, similarly sized particles pack into comparable void spaces without a fine fraction to interlock the matrix—about the worst combination possible for a steep slope under load.pack into similar-sized void spaces without an interlocking fine fraction to stiffen the matrix — the worst possible combination for a steep slope under load.

Table 2
Grain size distribution parameters from sieve analysis.

Sl.	D□□ (mm)	D□□ (mm)	D□□ (mm)	C_u	Cc	USCS
1	0.42	0.70	3.30	7.85	0.35	SP
2	0.41	0.70	3.30	8.04	0.36	SP
3	0.40	0.75	3.10	7.75	0.45	SP

Direct shear tests in CD condition returned cohesion values of 0.1–0.2 kPa—effectively cohesionless for any practical purpose—and friction angles of 32.7°–34.6° (Table 3;

Fig. 2). These sit at the lower end of the range Kainthola et al. [15] reported for comparable JCF dump materials, and fall somewhat below the 35°–38° typical of well-compacted granular fills [25]. The most likely explanation is the end-tipping placement method: material tipped over a crest tends to segregate, with coarser particles rolling to the toe and finer material concentrating near the crest, producing a compaction-deficient, weakly interlocked fabric [18].

Table 3
Geotechnical parameters from direct shear test and derived elastic constants.

Sl.	Sample	c' (kPa)	φ' (°)	ψ (°)	ν
1	Sample 1 (Top)	0.2	33.2°	22.1°	0.30
2	Sample 2 (Middle)	0.1	32.7°	21.8°	0.30
3	Sample 3 (Bottom)	0.2	34.6°	23.1°	0.30
—	Mean (± SD)	0.17 (± 0.06)	33.5° (± 1.0)	22.3° (± 0.7)	0.30

4.3 Deterministic Stability Analysis

4.3.1 LEM Results

The FOS values from all five LEM methods are collected in Table 4 and Fig. 3. Every method returns FOS < 1.0—the range runs from 0.751 (Janbu Simplified) to 0.770 (Janbu Corrected)—placing the slope consistently in failed-state territory. The spread across methods is only 0.019, indicating strong methodological convergence and ruling out any artefact of method choice. The slight underestimate from Janbu Simplified relative to the others is expected: without the empirical correction for inter-slice shear, the method tends to underpredict FOS by a few percent for slopes of this geometry [11].

To put these numbers in context: DGMS [34] sets an overall slope angle of 28° as a general safe limit for external OB dumps and prescribes a design FOS of 1.3. At 35°–38° and FOS ≈ 0.76, this slope is running at roughly 58% of the minimum acceptable safety margin. This is not a borderline case—it is a slope that should already be failing on theoretical grounds. That it hadn't visibly collapsed at the time of the September 2017 field investigation likely reflects transient suction effects in partially saturated coarse sand, which can provide 1–3 kPa of apparent cohesion under near-dry surface conditions [22, 23]. Once the monsoon fully saturates the fill, or sustained heavy rainfall eliminates that suction, the theoretical expectation of instability would be quickly realised.

Table 4
Factor of safety from deterministic LEM and FEM analyses.

Sl.	Method	Software	FOS	Stability
1	Bishop Simplified	LEM – SLIDE 6.0	0.764	Unstable
2	Morgenstern–Price	LEM – SLIDE 6.0	0.760	Unstable
3	Janbu Simplified	LEM – SLIDE 6.0	0.751	Unstable
4	Janbu Corrected	LEM – SLIDE 6.0	0.770	Unstable
5	Spencer	LEM – SLIDE 6.0	0.760	Unstable
6	FEM / SRM	FLAC/Slope 8.0	0.810	Unstable

4.3.2 FEM/SRM Results and Failure Mechanism

The FEM/SRM analysis in FLAC/Slope 8.0 returned FOS = 0.810—approximately 6% higher than the LEM average of 0.761. This pattern is commonly observed: FEM/SRM tends to return marginally higher FOS for simple homogeneous slopes because progressive stress redistribution allows partial load transfer away from the most critical zones, and because the failure mechanism is not pre-constrained to a circular arc—the kinematic constraints inherent in slice-based LEM can introduce a slight conservatism for planar or shallow-angle geometries [12, 24]. The difference is not large enough to alter the stability conclusion, but it serves as a useful cross-check. Where the FEM adds something the LEM cannot is in the spatial picture of failure: maximum shear strain rate concentration mapped to the mid-section of the slope, with secondary shear bands propagating toward the toe—consistent with the shallow rotational mechanism most commonly documented in end-tipped granular dumps [18, 25].

4.3.3 Effect of Friction Angle — Parametric Study

The parametric sweep over φ' = 29°–41° (Fig. 4) shows that LEM methods cross FOS = 1.0 at φ' ≈ 34°–35°, while FEM/SRM requires φ' ≈ 33°–34°. Given that measured field values fall at 32.7°–34.6°—directly straddling the stability boundary—the slope operates within a narrow margin of the critical friction angle. The practical implication is significant: even a modest reduction in φ' through saturation, weathering, or vibration-induced loosening could shift the slope from its current near-critical or sub-critical state into outright failure with limited warning.

The DGMS-recommended FOS of 1.3 [34] is not reached in the LEM until φ' reaches 38°–39°—some 4–5° above the field-measured mean. Achieving this through in-situ compaction alone would require a substantial increase in dry density. This is achievable in principle via mechanical rolling but operationally challenging on an already-constructed dump of 12–18 m height.

4.3.4 Effect of Cohesion — Parametric Study

The cohesion sweep (Fig. 5) tells a more encouraging story. Even a modest effective cohesion — say c' = 5 kPa — lifts the LEM FOS from approximately 0.72 to around 1.20. By c' = 10–15 kPa the slope satisfies FOS ≥ 1.3 in most LEM methods. These numbers are achievable: lime-stabilised mine spoil typically develops c' > 20 kPa within 28 days of treatment [19], and even biological soil crusts from early vegetation can contribute a few kPa of apparent cohesion through root binding. The nonlinearity at low c' values — where each additional kilopascal of cohesion produces a disproportionately large FOS gain — arises because cohesion appears in the numerator of the Mohr–Coulomb expression and acts uniformly along the entire slip surface, irrespective of depth [7, 25]. This has a straightforward engineering consequence: at very low cohesion levels (c' < 5 kPa), cohesion is actually the more *efficient* parameter to improve, in terms of FOS gain per unit of stabilisation effort, compared with friction angle.

5. Probabilistic Analysis

5.1 Monte Carlo Simulation Results

Table 5 and Fig. 6 present the full MCS results. Considering all three parameters as variable simultaneously (combined case, n = 100,000), the simulation returns $\mu_{FOS} = 0.764$—consistent with the deterministic result, as expected for symmetric distributions—with standard deviation $\sigma_{MCS} = 0.112$, giving $P^f \approx 98.3\%$ and $\beta = -2.29$. P_f is computed as $\Phi((1.0 - \mu_{FOS})/\sigma_{MCS}) = \Phi(2.107) \approx 98.3\%$, where $\sigma_{MCS} = 0.112$ is the standard deviation of the FOS distribution from the Monte Carlo trials. The reliability index $\beta = (\mu_{FOS} - 1.0)/\sigma_{FOSM} = (0.764 - 1.0)/0.103 = -2.29$ is derived independently via FOSM, using $\sigma_{FOSM} \approx 0.103$. These two estimates ($\sigma_{MCS} = 0.112$ and $\sigma_{FOSM} = 0.103$) are not interchangeable: σ_{MCS} reflects the full nonlinear FOS distribution from simulation, while σ_{FOSM} is a linearised approximation; the ~ 8% difference is expected and acceptable for the moderate CoV values here [28, 29]. The negative value $\beta = -2.29$ confirms the mean FOS lies 2.29 standard deviations below the failure threshold—the slope's expected state is failure. Assuming independent loading events each monsoon season, $P_f \approx 98\%$ per event implies near-certain failure over any multi-season mine life.

When only one parameter is varied at a time, the P^f values are 99.2% (φ' alone), 98.6% (c' alone), and 99.4% (γ alone)—all confirming the near-certain failure state. That the combined P_f (98.3%) is marginally lower than any single-parameter value reflects slight negative tail interaction when all parameters vary simultaneously at low CoV. This has a subtle implication: analyses that treat only one or two parameters probabilistically and fix the rest as deterministic produce P^f values within a few tenths of a percent of the fully

combined result in this case, though the principle—that partial probabilistic treatment can misrepresent total system P_f by several percentage points—holds more generally [28, 29].

Table 5

Summary of probabilistic analysis results: μ_FOS and σ_MCS from Monte Carlo Simulation; β = (μ_FOS − 1.0)/σ_FOSM from First-Order Second-Moment (FOSM) method — negative values indicate mean FOS lies below the failure threshold (β < 0 = failure-side); P_f from standard normal CDF using σ_MCS. Note: σ_MCS ≠ σ_FOSM; see § 5.1.

Analysis Case	N (trials)	μ_FOS	σ_MCS	P_f	β
φ' variable only (CoV = 6%)	10,000	0.764	0.098	99.2%	−2.41
c' variable only (CoV = 33%)	10,000	0.770	0.105	98.6%	−2.38
γ variable only (CoV = 5%)	10,000	0.767	0.092	99.4%	−2.46
All parameters combined	100,000	0.764	0.112	98.3%	−2.29

5.2 Sensitivity Analysis

The tornado diagram (Fig. 7) ranks six input parameters by their ± 1σ influence on FOS. Friction angle leads by a clear margin (ΔFOS = + 0.185 for + 1σ), followed by slope height (− 0.142 for + 1σ increase), cohesion (+ 0.128), unit weight, pore water pressure, and slope angle in decreasing order. Friction angle's dominance over cohesion might at first seem to contradict the cohesion parametric study. The resolution is straightforward: the ± 1σ perturbation for φ' is ± 2° (6% CoV × 33.5°), while for c' it is only ± 0.05 kPa (33% CoV × 0.15 kPa)—a tiny absolute increment that barely moves the FOS. Reframe the question as 'which parameter, improved by 10 kPa, gives the largest FOS gain?' and cohesion wins clearly. Context matters when interpreting sensitivity analyses [1, 6].

5.3 Reliability–FOS Design Chart

Figure 8 plots β against μ_FOS for CoV values of 0.10 to 0.25. The current slope sits at (μ_FOS = 0.764, β = −2.29)—in the unacceptable failure zone, with Pf ≈ 98%. The chart is most useful as a design tool for evaluating remediated conditions: to reach the safe-side minimum of β = +3.0 with CoV ≈ 0.20, mean FOS would need to reach roughly 1.60. Alternatively, cutting CoV from 0.20 to 0.10 through a more intensive site investigation programme lowers the required mean FOS to approximately 1.30 for the same β = +3.0 target. This illustrates that investment in characterisation quality can, in effect, reduce the structural intervention required to satisfy a reliability criterion.

6. Discussion

Five LEM methods, one FEM analysis, and a 100,000-trial Monte Carlo simulation all converge on the same verdict: this slope is critically unstable and carries a near-certain probability of failure under current conditions. The practical message is unambiguous—this is not a borderline situation requiring further study before action; it is a slope already in its expected failure state, warranting immediate remediation.

What is perhaps more analytically interesting is what the data reveal about *why* the slope is so marginal. The end-tipping construction method has produced fill with $\varphi' \approx 33.5°$—4–5° below what would normally be targeted for a stable slope of this height and angle. Near-zero cohesion means there is no reserve strength to draw on during transient loading events: a 50 mm rainfall episode, a blast vibration from an adjacent working, or the gradual saturation front advancing through the fill during a prolonged wet season could all push the slope across the failure threshold without warning. The FLAC analysis's identification of maximum shear strain at mid-slope is consistent with the progressive failure pattern documented in the Lalmatia and Sesti incidents [17, 41], where initial toe distress propagated rapidly upward.pattern documented in the Lalmatia and Sesti incidents [17, 41], where initial toe distress propagated rapidly upward.

The probabilistic analysis adds something the deterministic picture alone cannot provide. A Pf of roughly 98.3% from the combined MCS—far beyond the commonly accepted 2.3% threshold corresponding to $\beta_target = +2.0$ [28]—means virtually the entire distribution of possible FOS values lies inside the failure zone. Even optimistic combinations of input parameters (say, $+1\sigma$ in both φ' and c' simultaneously) yield FOS only around 0.96—still below unity. No plausible combination of high-end material properties produces stability under the current slope geometry.

The finding that more intensive site investigation—reducing CoV from 0.20 to 0.10—can lower the required mean FOS from 1.60 to 1.30 for the same β target deserves particular attention from mine operators. Routine geotechnical investigation in Indian opencast mines often rests on a handful of index property tests and, at best, a single consolidated-undrained triaxial test. The CoV of φ' from such sparse datasets is inevitably high. A campaign of ten to fifteen direct shear or triaxial tests per dump would likely halve the coefficient of variation and substantially close the gap between current performance and the reliability target—at a fraction of the cost of physical remediation.

On stabilisation options, the cohesion parametric study suggests that chemical treatment—lime, Portland cement, or approaches such as enzyme-induced calcite precipitation—offers the steepest FOS gain per unit cost at the current near-zero baseline. A cohesion increase to 10–15 kPa, achievable with 3–5% lime admixture in sandy soils [19], would push mean FOS above 1.3 without touching the slope geometry. Reducing slope angle to $\leq 28°$ (as DGMS [34] requires) remains the most robust long-term fix, but means re-

handling already-placed waste—an operational and economic commitment that mine management often resists. The design chart in Fig. 8 can be a useful tool in that conversation: it shows precisely what FOS is needed for a given risk tolerance, which tends to be a more tractable discussion with management than an abstract reliability index. The normalised cross-comparison of geotechnical and physico-chemical properties across the three samples (Fig. 9) confirms the remarkable uniformity of the fill material, supporting the use of a single-slope model as representative of the broader dump profile.

6.1 International Context and Framework Transferability

Although the field evidence comes from the JCF, the integrated framework presented here is not geographically constrained. End-tipped overburden dumps built from loosely consolidated granular fill feature in opencast mining operations worldwide: in the Bowen Basin (Australia), the Powder River Basin (USA), the lignite fields of Eastern Europe, and the rapidly expanding coalfields of Indonesia and Mozambique. The common thread is low cohesion, moderate friction angle, and placement geometry that routinely exceeds the geomechanically defensible stable angle—precisely the conditions studied here. The three-stage framework (physico-chemical characterisation → multi-method deterministic analysis → probabilistic risk quantification with design chart) is structured to work from standard laboratory inputs available at any mine site, requires no specialist probabilistic software beyond a Monte Carlo implementation in any scripting environment, and produces output—the β–FOS design chart—that maps directly onto existing regulatory frameworks including DGMS (India), applicable Australian state mining authorities (e.g., DMIRS in Western Australia, DERM in Queensland), and MSHA (USA) performance standards. Applying the same framework across a wider portfolio of dump geometries, fill lithologies, and climatic settings would allow the FOS-to-β conversion chart to be generalised into a regional or global nomograph for OB dump risk screening—a practically valuable outcome for mine permitting and closure planning.

6.2 Limitations and Future Work

One limitation of this study that warrants acknowledgement is the use of a simplified closed-form Bishop expression inside the Monte Carlo loop rather than the full iterative LEM solver. This is a common practical compromise [1, 29], but it means the MCS does not capture the inter-slice force interactions that, in a more rigorous treatment, would slightly modify the shape of the FOS distribution. For the low-cohesion, steep-slope geometry studied here, the error is probably small—well within the uncertainty attributable to CoV assumptions—but future work using faster LEM implementations embedded in probabilistic engines (e.g., the probabilistic mode in SLIDE 6.0 or GeoStudio SLOPE/W) would be valuable for verification. Separately, this study treats pore water

pressures as deterministic; incorporating a spatial rainfall-infiltration model coupled to a transient FEM slope stability analysis, as demonstrated by Bittelli et al. [21] and Gavin & Xue [22], would provide a more complete picture of monsoon-season risk.

7. Conclusions

This study developed and field-tested an integrated geotechnical–probabilistic–environmental risk assessment framework for mine overburden dump slopes, applied to a representative case in the Eastern Jharia Coalfield. The framework links physico-chemical fill characterisation, multi-method deterministic stability analysis, and Monte Carlo–based probabilistic risk quantification into a coherent, repeatable methodology. The main conclusions are as follows:

(1) All five LEM methods and the FEM/SRM analysis classify the studied OB dump slope as critically unstable (FOS = 0.751–0.810), operating at roughly 58% of the DGMS minimum design standard of FOS = 1.3. The consistency across methods removes any methodological ambiguity from this conclusion.

(2) Monte Carlo Simulation (n = 100,000) returns a probability of failure of approximately 98% and reliability index $\beta = -2.29$ (negative sign confirming the mean FOS lies on the failure side of the limit state) — well above the commonly accepted 2.3% threshold corresponding to $\beta_{target} = +2.0$, indicating near-certain failure under current conditions. Treating the slope instability as only a deterministic problem misses the full probabilistic context that quantifies this certainty.

(3) Friction angle is the dominant input parameter in sensitivity analysis, but cohesion offers the most efficient remediation leverage at the current near-zero baseline: FOS > 1.3 is achievable with $c' \geq 10$–15 kPa, attainable through lime or cement stabilisation of the fill [19].

(4) The design chart relating β to mean FOS across a range of CoV values (Fig. 8) illustrates that improved site characterisation — reducing CoV from 0.20 to 0.10 — lowers the mean FOS required to achieve $\beta = +3.0$ from approximately 1.60 to 1.30, enabling more economical structural interventions to meet the reliability target.

(5) The dump material (USCS classification SP) is physico-chemically unsuitable for direct revegetation, requiring soil amendment to address low pH, deficient macro-nutrients, and trace heavy metal contamination — particularly elevated mercury likely linked to subsurface mine-fire activity in the JCF.

(6) The integrated framework — physico-chemical characterisation, multi-method deterministic analysis, and MCS-based probabilistic risk quantification culminating in a β–

FOS design chart — requires only standard site investigation inputs and is directly transferable to OB dump assessment at any opencast mine globally. Embedding this framework within mine permitting, closure planning, and regulatory compliance workflows would represent a material advance over prevailing deterministic-only practice in several coal-producing nations.

8. Scope for Future Work

Several threads from this work merit further investigation. The most pressing is transient pore water pressure modelling—coupled rainfall-infiltration–stability analysis is needed to characterise the full seasonal risk envelope, given that the most critical conditions clearly occur during and after monsoon events. Dynamic stability under blast-induced vibration from adjacent working faces is another gap: at the slope dimensions and material properties observed here, even modest peak particle velocities could tip an already-marginal slope into failure. Field-scale nail pull-out testing would ground-truth the soil nailing option, which conceptually appears well-suited to providing immediate cohesion-equivalent resistance in near-cohesionless fill. On the ecological side, a longitudinal study tracking revegetation success under different soil amendment regimes—monitoring both surface stability indicators and vegetation cover over time—would strengthen the evidence base for post-mining reclamation standards in the JCF.different soil amendment regimes — tracking both surface stability indicators and vegetation cover evolution — would strengthen the evidence base for post-mining reclamation standards in the JCF context.

Declarations

Author Contribution

All the authors have contributed equally.

Data Availability

Laboratory data supporting the findings of this study are available from the corresponding author upon reasonable request.

References

1. Malkawi, A.I.H., Hassan, W.F., & Abdulla, F.A. (2000). Uncertainty and reliability analysis applied to slope stability. Structural Safety, 22(2), 161–187.
2. Wu, T.H., & Kraft, L.M. (1970). Safety analysis of slopes. Journal of the Soil Mechanics and Foundations Division, ASCE, 96(2), 609–630.

3. Alonso, E.E. (1976). Risk analysis of slopes and its application to slopes in Canadian Geotechnique. Canadian Geotechnical Journal, 13(3), 201–215.
4. Tang, W.H., Yucemen, M.S., & Ang, A.H.S. (1976). Probability-based short-term design of slopes. Canadian Geotechnical Journal, 13(3), 201–215.
5. Vanmarcke, E.H. (1977). Reliability of earth slopes. Journal of Geotechnical Engineering Division, ASCE, 103(11), 1227–1246.
6. Cornell, C.A. (1971). First-order uncertainty analysis of soil deformation and stability. Proc. 1st ICASP Conference, Hong Kong, 129–144.
7. Bishop, A.W. (1955). The use of the slip circle in the stability analysis of slopes. Géotechnique, 5(1), 7–17.
8. Morgenstern, N.R., & Price, V.E. (1965). The analysis of the stability of general slip surfaces. Géotechnique, 15(1), 79–93.
9. Spencer, E. (1967). A method of analysis of the stability of embankments assuming parallel inter-slice forces. Géotechnique, 17(1), 11–26.
10. Janbu, N. (1954). Application of composite slip surfaces for stability analysis. Proc. European Conf. on Stability of Earth Slopes, Stockholm, 3, 43–49.
11. Fredlund, D.G., & Krahn, J. (1977). Comparison of slope stability methods of analysis. Canadian Geotechnical Journal, 14(3), 429–439.
12. Hammah, R., Yacoub, T., Corkum, B., & Curran, J. (2005). A comparison of finite element slope stability analysis with conventional limit-equilibrium investigation. Proc. 58th Canadian Geotechnical Conference (GeoSask).
13. Aryal, K.P. (2006). Slope stability evaluations by limit equilibrium and finite element methods. Doctoral Thesis, NTNU, Norway.
14. Steiakakis, E., Kavouridis, K., & Monopolis, D. (2009). Large scale failure of the external waste dump at the "South Field" lignite mine, Northern Greece. Engineering Geology, 104(3–4), 269–279.
15. Kainthola, A., Verma, D., Gupte, S.S., & Singh, T.N. (2011). A coal mine dump stability analysis — a case study. Geomaterials, 1(1), 1–13.
16. Poulsen, B., Khanal, M., Rao, A.M., Adhikary, D., & Balusu, R. (2014). Mine overburden dump failure: A case study. Geotechnical and Geological Engineering, 32(2), 297–309.
17. Rai, A.K., Paul, B., & Singh, G. (2011). A study on physico-chemical properties of overburden dump materials from selected coal mining areas of Jharia coalfields. Advances in Applied Science Research, 2(2), 122–132.
18. Dawson, R.F., Morgenstern, N.R., & Stokes, A.W. (1998). Liquefaction flowslides in rocky mountain coal mine waste dumps. Canadian Geotechnical Journal, 35(2), 328–343.

19. Ulusay, R., Ekmekci, M., Tuncay, E., & Nalbantoğlu, N. (2014). Improvement of slope stability based on integrated geotechnical evaluations at a lignite open pit. Engineering Geology, 181, 261–280.
20. Rosengren, K., Simmons, J., & Maconochie, A.P. (2010). Geotechnical investigations for open pit mines — 250 m and beyond. Bowen Basin Symposium, 169–179.
21. Bittelli, M., Valentino, R., Salvatorelli, F., & Pisa, P.R. (2012). Monitoring soil–water and displacement conditions leading to landslide occurrence in partially saturated clays. Geomorphology, 173–174, 161–173.
22. Gavin, K., & Xue, J. (2008). A simple method to analyse infiltration into unsaturated soil slopes. Computers and Geotechnics, 35(2), 223–230.
23. Batali, L., & Andreea, C. (2016). Slope stability analysis using the unsaturated stress analysis: Case study. Procedia Engineering, 143, 284–291.
24. Yu, H.S., Salgado, R., Sloan, S.W., & Kim, J.M. (1998). Limit analysis versus limit equilibrium for slope stability. Journal of Geotechnical and Geoenvironmental Engineering, 124(1), 1–11.
25. Abramson, L.W., Lee, T.S., Sharma, S., & Boyce, G.M. (2002). Slope stability and stabilization methods (2nd ed.). Wiley-Interscience.
26. Low, B.K., & Tang, W.H. (1997). Efficient reliability evaluation using spreadsheet. Journal of Engineering Mechanics, 123(7), 749–752.
27. Hassan, A.M., & Wolff, T.F. (1999). Search algorithm for minimum reliability index of earth slopes. Journal of Geotechnical and Geoenvironmental Engineering, 125(4), 301–308.
28. Christian, J.T., Ladd, C.C., & Baecher, G.B. (1994). Reliability applied to slope stability analysis. Journal of Geotechnical Engineering, 120(12), 2180–2207.
29. El-Ramly, H., Morgenstern, N.R., & Cruden, D.M. (2002). Probabilistic slope stability analysis for practice. Canadian Geotechnical Journal, 39(3), 665–683.
30. Maiti, S.K., Karmakar, N.C., & Sinha, I.N. (2002). Studies on some physical parameters aiding biological reclamation of mine spoil dump — Jharia coalfield. International Mining Engineering Journal.
31. Chaulya, S.K., Singh, R.S., Chakraborty, M.K., & Tewary, B.K. (2000). Bioreclamation of coal mine overburden dumps in India. Land Contamination & Reclamation, 8(2), 117–129.
32. Rai, P.B., & Mahapatra, S. (2013). Overburden dump slope stability: A case study at a coal mine. Dept. of Mining Engineering, NIT Rourkela.
33. Richards, B.G., Coulthard, M.A., & Toh, C.T. (1981). Analysis of slope stability at Goonyella Mine. Canadian Geotechnical Journal, 18(2), 179–194.

34. DGMS (2003). Circular No. 05 — Safety standards for slope stability in opencast mines. Ministry of Labour, Government of India.
35. Parmar, T.D., & Dave, S.P. (2015). Software used in slope stability analysis. International Journal for Scientific Research & Development, 2(12), 576–580.
36. Sengupta, N. (1980). A revision of the geology of the Jharia coalfield. PhD Thesis, ISM Dhanbad, India.
37. Phoon, K.K., & Kulhawy, F.H. (1999). Characterisation of geotechnical variability. Canadian Geotechnical Journal, 36(4), 612–624.
38. Brady, N.C., & Weil, R.R. (2008). The Nature and Properties of Soils (14th ed.). Pearson Prentice Hall, Upper Saddle River, NJ.
39. Saxena, A.K., & Chandrasekaran, B. (2003). Soil quality management and reclamation of degraded land. In: Proc. International Symposium on Soil Degradation and Reclamation, New Delhi, India.
40. Obrzud, R., & Truty, A. (2012). The Hardening Soil Model: A Practical Guidebook. Zace Services Ltd., Switzerland.
41. DGMS (2016). Investigation Report on Overburden Dump Collapse at Lalmatia Opencast Project, Eastern Coalfields Limited, Rajmahal, Jharkhand — 29 September 2016. Directorate General of Mines Safety, Ministry of Labour and Employment, Government of India, Dhanbad.

Figures

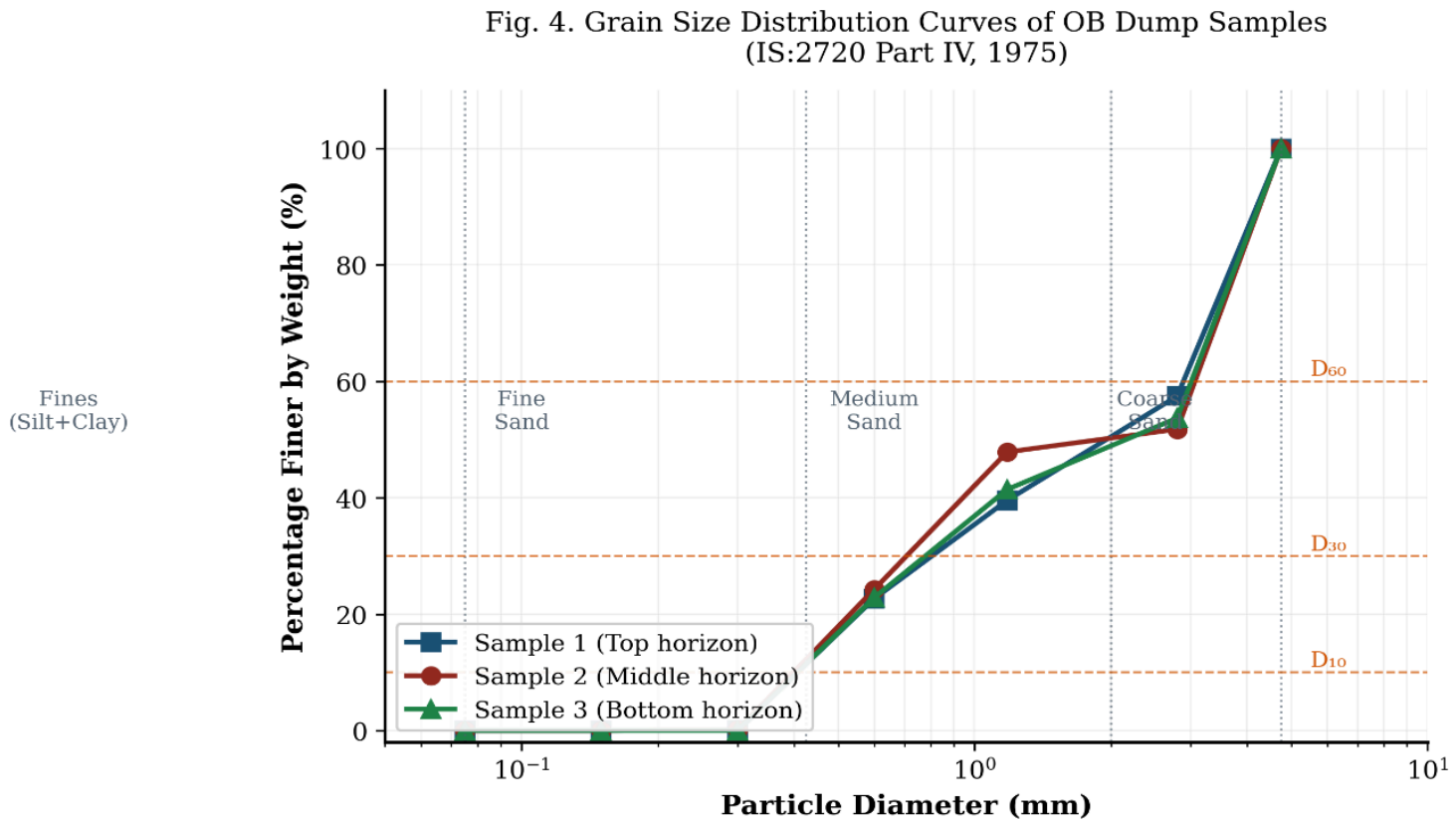


Figure 1

Grain size distribution curves for the three OB dump samples (IS:2720 Part IV, 1985).

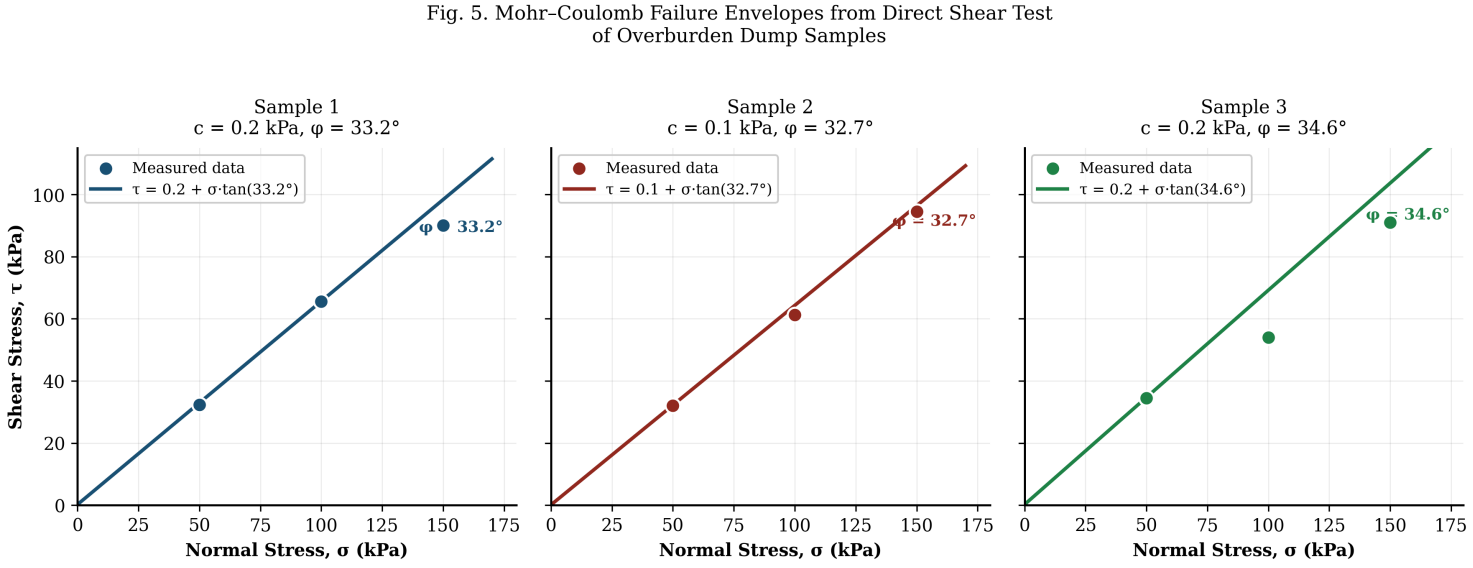


Figure 2

Mohr–Coulomb failure envelopes from consolidated-drained direct shear tests on three OB dump samples.

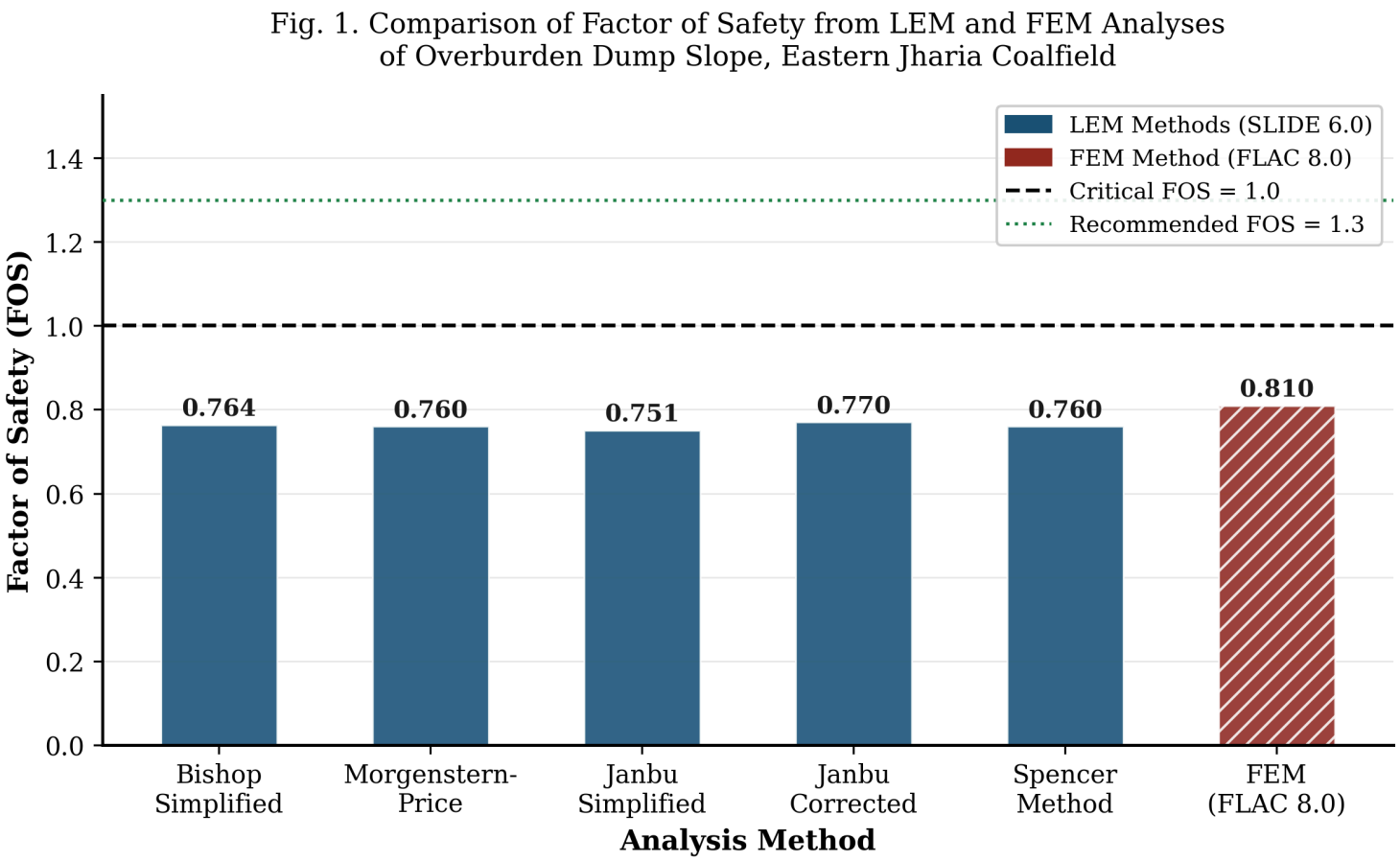


Figure 3

Comparison of FOS from LEM (SLIDE 6.0) and FEM (FLAC/Slope 8.0) analyses of the OB dump slope.

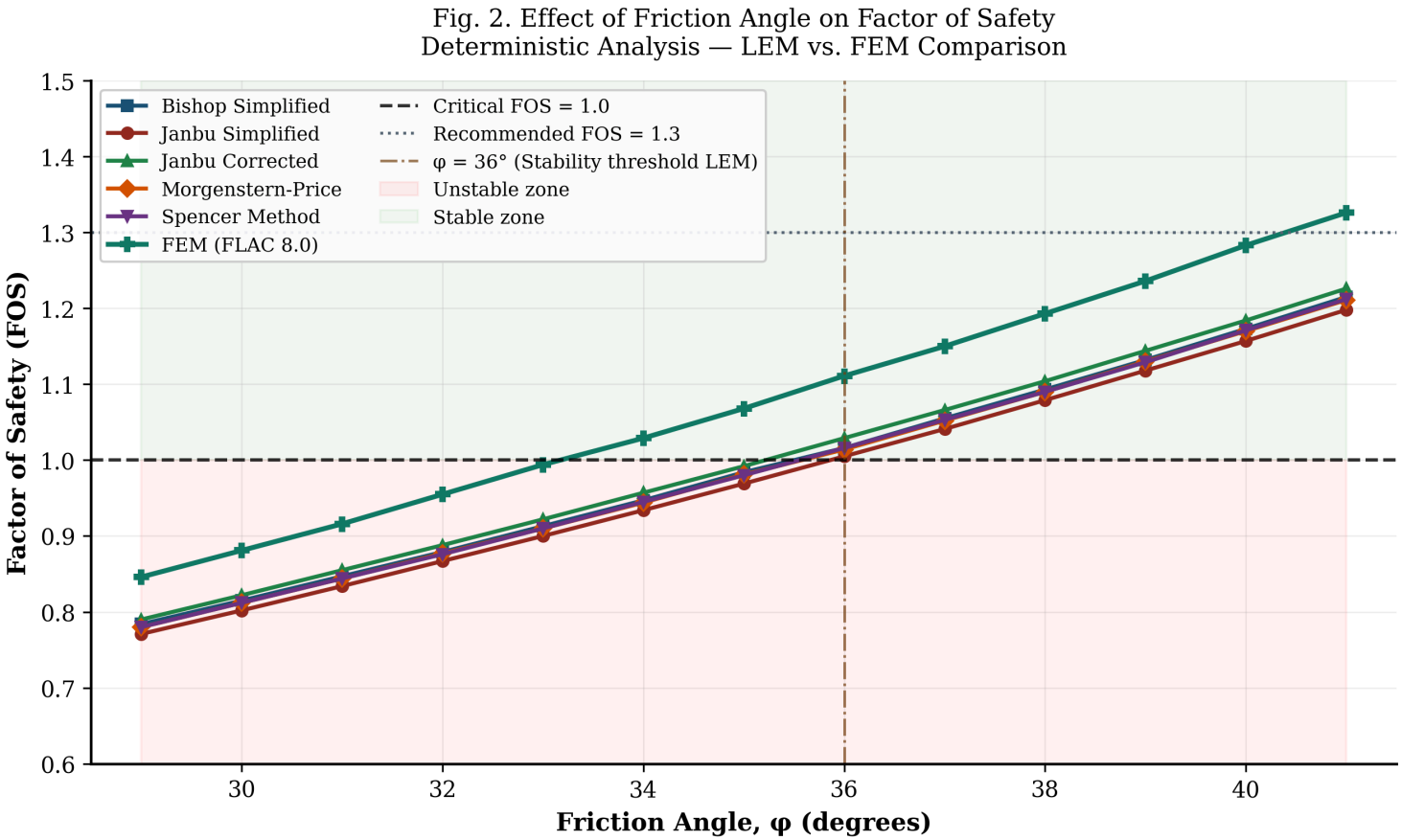


Figure 4

Parametric study: effect of friction angle on factor of safety — LEM vs. FEM comparison.

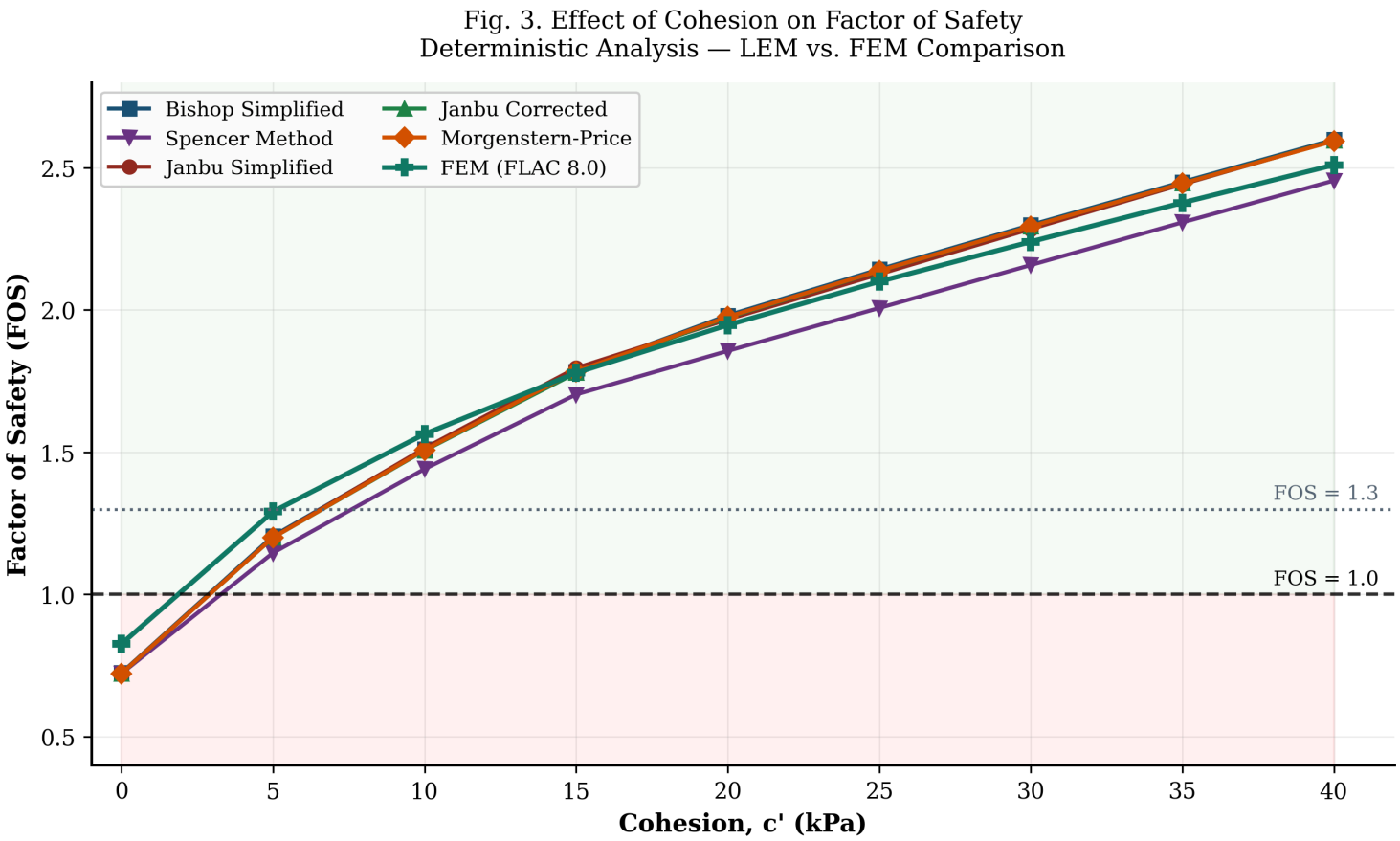


Figure 5

Parametric study: effect of cohesion on factor of safety — LEM vs. FEM comparison.

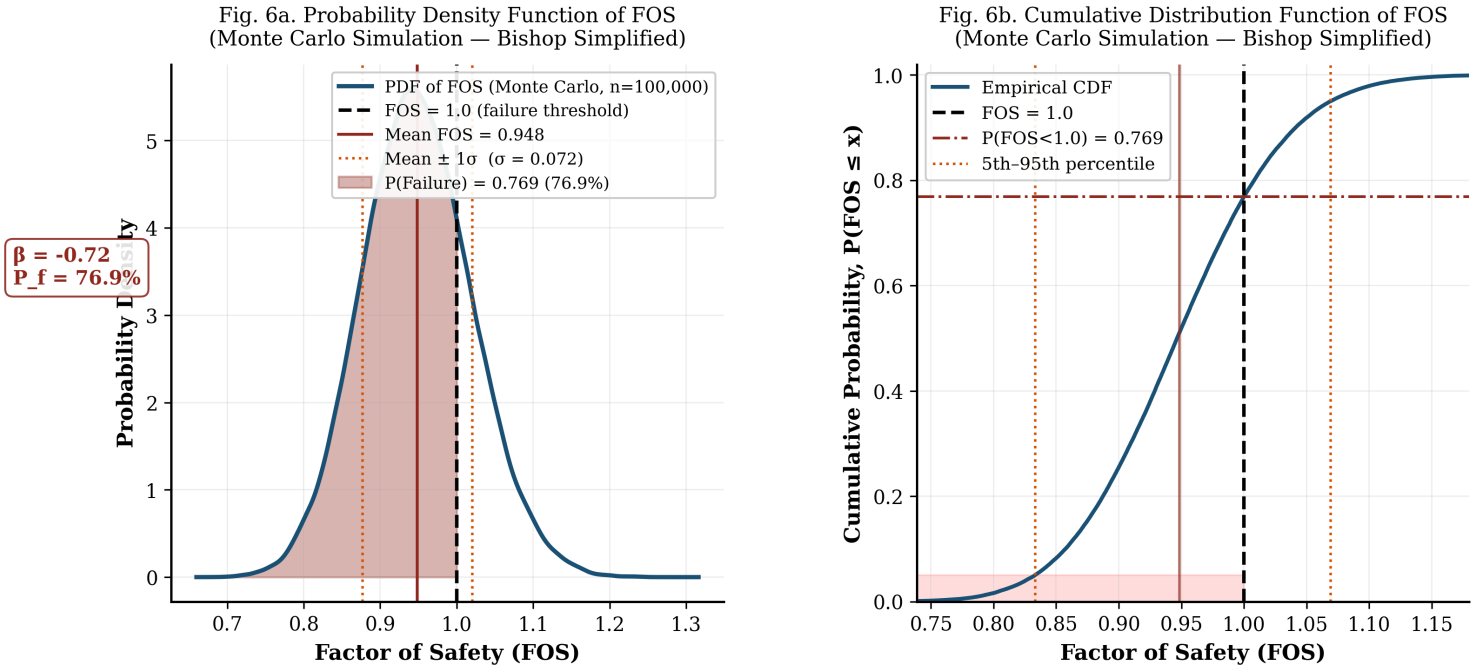


Figure 6

(a) Probability density function and (b) cumulative distribution function of FOS from Monte Carlo Simulation (n = 100,000; Bishop Simplified basis).

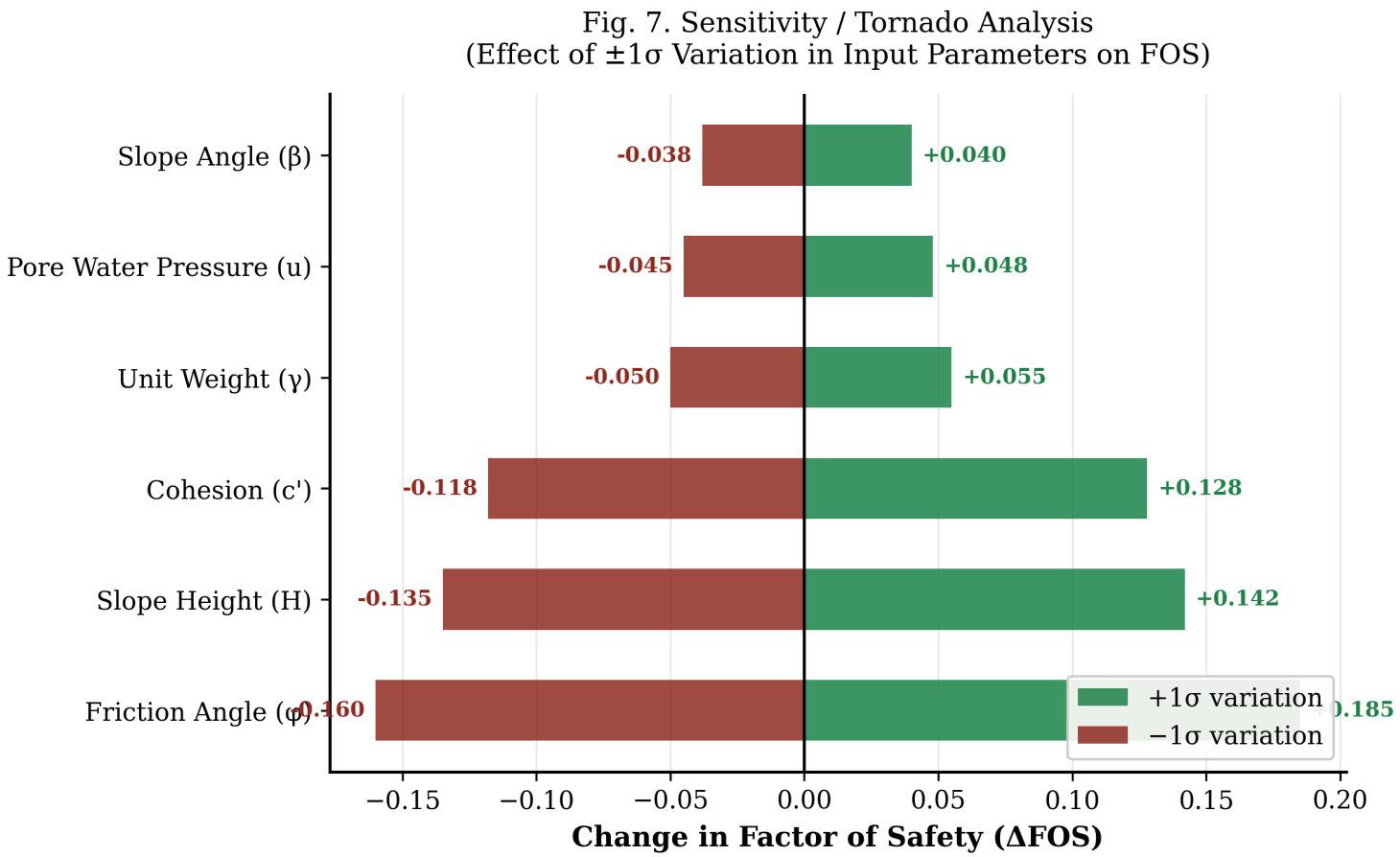


Figure 7

Tornado (sensitivity) diagram showing the effect of ±1σ variation in key input parameters on factor of safety.

Fig. 8. Relationship Between Reliability Index (β) and Mean FOS
for Different Coefficients of Variation (CoV)

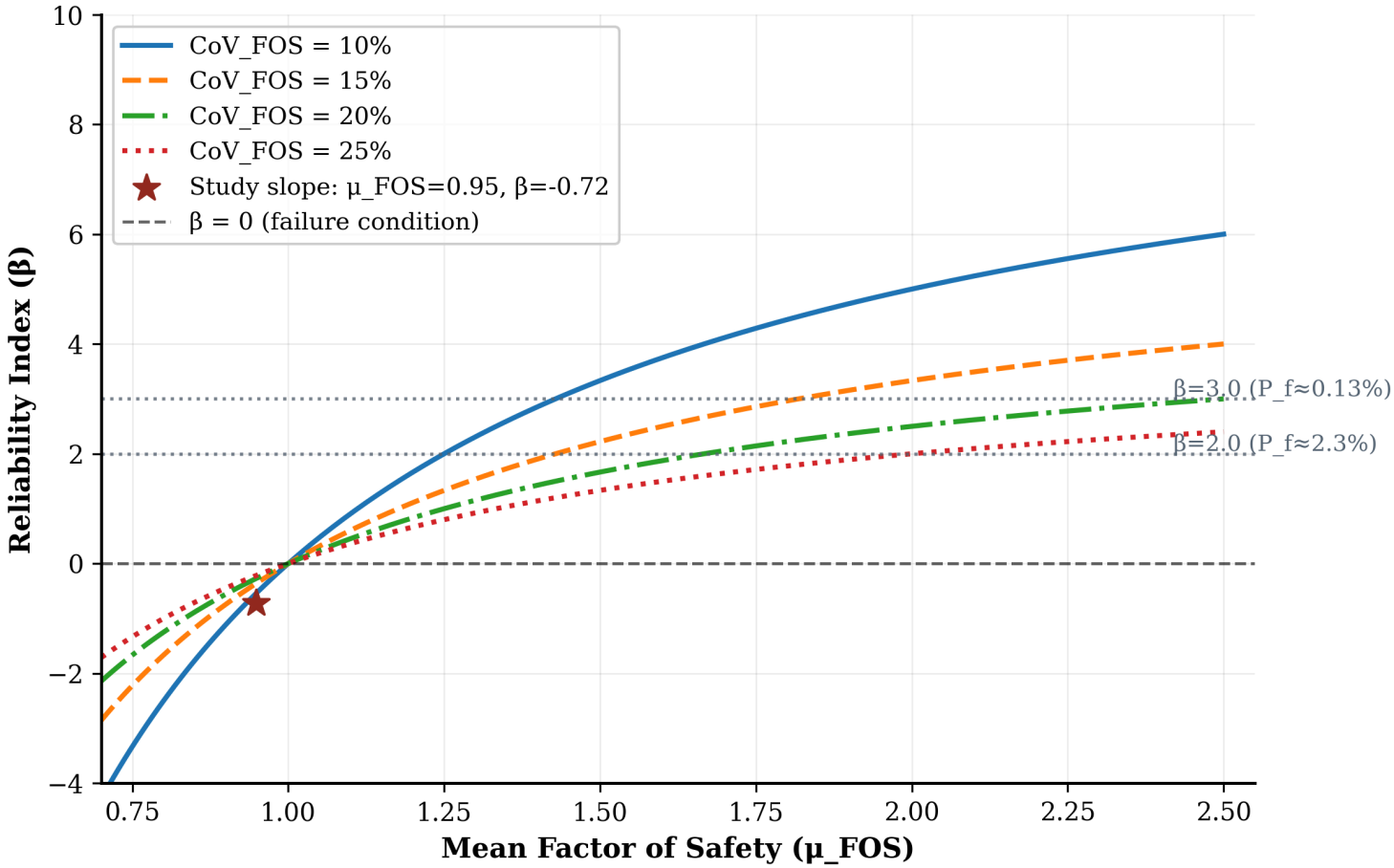


Figure 8

Design chart: reliability index (β) as a function of mean FOS for varying CoV — practical tool for probabilistic slope assessment.

Fig. 9. Comparative Geotechnical and Physico-Chemical Properties of OB Dump Samples (Normalized)

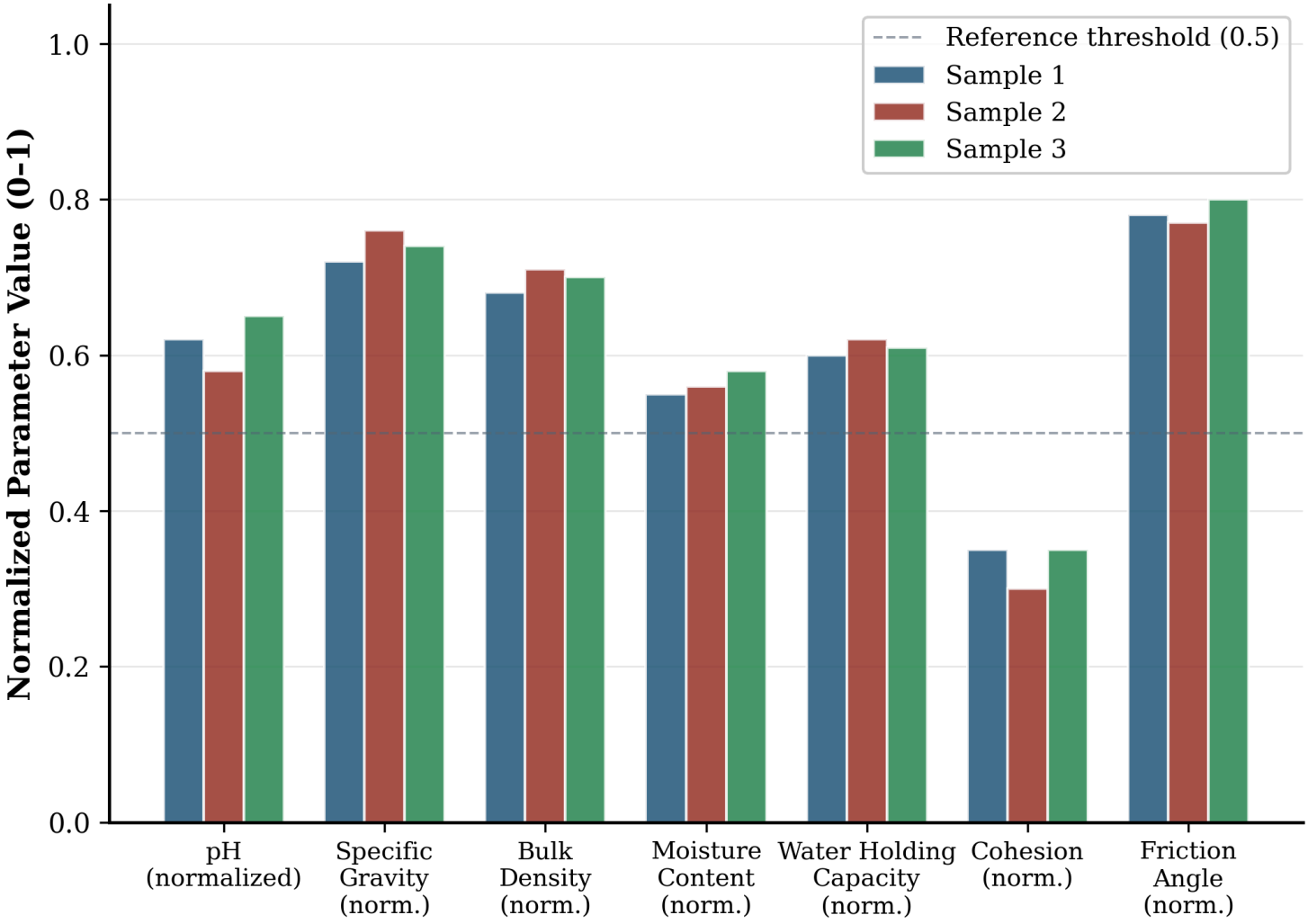


Figure 9

Normalised geotechnical and physico-chemical comparison of the three OB dump samples.